

RESEARCH ARTICLE

# Ligand Binding to the FA3-FA4 Cleft Inhibits the Esterase-Like Activity of Human Serum Albumin

Paolo Ascenzi<sup>1\*</sup>, Loris Leboffe<sup>2</sup>, Alessandra di Masi<sup>2</sup>, Viviana Trezza<sup>2</sup>, Gabriella Fanali<sup>3</sup>, Magda Gioia<sup>4,5</sup>, Massimo Coletta<sup>4,5</sup>, Mauro Fasano<sup>3</sup>

**1** Interdepartmental Laboratory of Electron Microscopy, Roma Tre University, Via della Vasca Navale 79, I-00146 Roma, Italy, **2** Department of Sciences, Roma Tre University, Viale Guglielmo Marconi 446, I-00146 Roma, Italy, **3** Biomedical Research Division, Department of Theoretical and Applied Sciences, University of Insubria, Via Alberto da Giussano 12, I-21052 Busto Arsizio (VA), Italy, **4** Department of Clinical Sciences and Translational Medicine, University of Roma "Tor Vergata", Via Montpellier 1, I-00133 Roma, Italy, **5** Interuniversity Consortium for the Research on the Chemistry of Metals in Biological Systems, Via Celso Ulpiani 27, I-70126 Bari, Italy

\* [ascenzi@uniroma3.it](mailto:ascenzi@uniroma3.it)



## OPEN ACCESS

**Citation:** Ascenzi P, Leboffe L, di Masi A, Trezza V, Fanali G, Gioia M, et al. (2015) Ligand Binding to the FA3-FA4 Cleft Inhibits the Esterase-Like Activity of Human Serum Albumin. PLoS ONE 10(3): e0120603. doi:10.1371/journal.pone.0120603

**Academic Editor:** Eugene A. Permyakov, Russian Academy of Sciences, Institute for Biological Instrumentation, RUSSIAN FEDERATION

**Received:** November 6, 2014

**Accepted:** January 24, 2015

**Published:** March 19, 2015

**Copyright:** © 2015 Ascenzi et al. This is an open access article distributed under the terms of the [Creative Commons Attribution License](https://creativecommons.org/licenses/by/4.0/), which permits unrestricted use, distribution, and reproduction in any medium, provided the original author and source are credited.

**Data Availability Statement:** All relevant data are within the paper and its Supporting Information files.

**Funding:** This work was supported by Ministero dell'Istruzione, dell'Università e della Ricerca of Italy (Università Roma Tre, Roma, Italy; CLAR 2014 to PA) and Consorzio Interuniversitario Italiano per l'Argentina (CUIA 2014 to PA). The funders had no role in study design, data collection and analysis, decision to publish, or preparation of the manuscript.

**Competing Interests:** The authors have declared that no competing interests exist.

## Abstract

The hydrolysis of 4-nitrophenyl esters of hexanoate (NphOHe) and decanoate (NphODE) by human serum albumin (HSA) at Tyr411, located at the FA3-FA4 site, has been investigated between pH 5.8 and 9.5, at 22.0°C. Values of  $K_s$ ,  $k_{+2}$ , and  $k_{+2}/K_s$  obtained at  $[HSA] \geq 5 \times [NphOXx]$  and  $[NphOXx] \geq 5 \times [HSA]$  (Xx is NphOHe or NphODE) match very well each other; moreover, the deacylation step turns out to be the rate limiting step in catalysis (*i.e.*,  $k_{+3} \ll k_{+2}$ ). The pH dependence of the kinetic parameters for the hydrolysis of NphOHe and NphODE can be described by the acidic  $pK_a$ -shift of a single amino acid residue, which varies from 8.9 in the free HSA to 7.6 and 7.0 in the HSA:NphOHe and HSA:NphODE complex, respectively; the  $pK_a$ -shift appears to be correlated to the length of the fatty acid tail of the substrate. The inhibition of the HSA-Tyr411-catalyzed hydrolysis of NphOHe, NphODE, and 4-nitrophenyl myristate (NphOMy) by five inhibitors (*i.e.*, diazepam, diflunisal, ibuprofen, 3-indoxyl-sulfate, and propofol) has been investigated at pH 7.5 and 22.0°C, resulting competitive. The affinity of diazepam, diflunisal, ibuprofen, 3-indoxyl-sulfate, and propofol for HSA reflects the selectivity of the FA3-FA4 cleft. Under conditions where Tyr411 is not acylated, the molar fraction of diazepam, diflunisal, ibuprofen, and 3-indoxyl-sulfate bound to HSA is higher than 0.9 whereas the molar fraction of propofol bound to HSA is ca. 0.5.

## Introduction

The (pseudo-)enzymatic activity of human serum albumin (HSA) was first reported in 1951 and investigated extensively for decades. Among others, HSA displays esterase, RNA-hydrolyzing, enolase, glucuronidase, lipid peroxidase, aldolase glutathione-linked thiol peroxidase, and

anti-oxidant activities. Moreover, heme binding confers to HSA globin-like (pseudo-)enzymatic properties, including detoxification of reactive nitrogen and oxygen species as well as catalase and peroxidase activities. Remarkably, HSA(-heme) (pseudo-)enzymatic properties are modulated allosterically and inhibited competitively [1,2].

Although the physiological importance of the esterase activity of HSA is obscure and the natural substrates are still unknown, HSA displays esterase activity towards several substrates including 4-nitrophenyl acetate (NphOAc),  $\alpha$ -naphthyl acetate, phenyl acetate, 1-naphthyl *N*-methylcarbamate,  $\beta$ -naphthyl acetate, aspirin, ketoprofen glucuronide, carprofen acylglucuronide, cyclophosphamide, nicotinate esters, long and short-chain FA esters (e.g., 4-nitrophenyl myristate; NphOMy), octanoyl ghrelin, organophosphorus pesticides, carbaryl, 2-nitrotrifluoroacetanilide, 2-nitroacetanilide, and nerve agents [1–3].

The Lys199 and Tyr411 residues, placed in the fatty acid (FA) 7 (FA7) and 3–4 (FA3-FA4) site, respectively, are pivotal for the esterase activity of HSA; however, mechanisms for the Lys199- and Tyr411-assisted catalysis are substantially different [1–8].

At Lys199, the substrate (e.g., acetylsalicylic acid, trinitrobenzeno-sulfonates, and penicillin) is cleaved in two products; while one product is released, the other one binds covalently to the Lys199 residue [1,4,7]. Although the molecular mechanism underlying the Lys199 acetylation is unknown, it seems that its ability to attack the substrate is due to the proximity of the Lys195 residue, these two residues playing a combined and comparable chemical role. In fact, the basic form of Lys199 is likely connected to the acid form of Lys195 through a network of H-bonding water molecules with a donor-acceptor character. The presence of these water bridges is relevant for stabilizing the configuration of the FA7 site and/or promoting a potential Lys195–Lys199 proton-transfer process [6]. Since Lys199 is placed at the entrance of the FA7 site (i.e., Sudlow's site I), ligand binding inhibits the Lys199-dependent esterase activity [3,8].

The catalytic mechanism involving the Tyr411 residue appears to be substrate-dependent. Of note, the hydrolysis of the most suitable substrate 4-nitrophenyl propionate leads to the release of both 4-nitrophenol and propionate [9]. This mechanism also applies to the hydrolysis of *N*-trans-cinnamoylimidazoles [10] and 4-nitrophenyl esters of amino acids [11]. However, the Tyr411-assisted hydrolysis of NphOAc and NphOMy leads to the release of 4-nitrophenol and to Tyr411-acetylation and -myristoylation, respectively [12,13]. The strong nucleophilic nature of the phenolic oxygen of the Tyr411 residue is due to the close proximity of the Arg410 guanidine moiety that electrostatically stabilizes the reactive anionic form of the Tyr411 residue [5,14]. Since both the Arg410 and Tyr411 residues are placed in the FA3-FA4 site (i.e., Sudlow's site II), ligand binding inhibits the HSA esterase activity [3,9,12,13]. Remarkably, the esterase activity of HSA could play a role in the inactivation of several toxins including organophosphorus compounds [3].

Present study largely extends previous investigations concerning the hydrolysis of 4-nitrophenyl esters by HSA [9,12–14]. In particular, kinetics of the HSA pseudo-enzymatic hydrolysis of 4-nitrophenyl hexanoate (NphOHe) and 4-nitrophenyl decanoate (NphODE) have been investigated between pH 5.8 and 9.5, under conditions where  $[HSA] \geq 5 \times [NphOXx]$  and  $[NphOXx] \geq 5 \times [HSA]$  (Xx indicates He or De). The rationale behind this selection is to investigate how the FA tail length affects the  $pK_a$  values of the ionizing group that modulates the catalysis. Furthermore, diazepam, diflunisal, ibuprofen, 3-indoxyl-sulfate, and propofol have been reported to inhibit competitively the HSA-Tyr411-catalyzed hydrolysis of NphOHe, NphODE, and 4-nitrophenyl myristate (NphOMy) (see [12] and present study). Remarkably, the molar fraction of diazepam, diflunisal, ibuprofen, and 3-indoxyl-sulfate bound to not acylated HSA is higher than 0.9 whereas the molar fraction of propofol bound to HSA is *ca.* 0.5.

## Materials and Methods

NphOHe, NphODE, NphOMy, 4-nitrophenol (NphOH), diazepam, diflunisal, ibuprofen, 3-indoxyl-sulfate, propofol, and 1,3-bis(tris(hydroxymethyl)methylamino)propane (Bis-tris propane) were obtained from Sigma-Aldrich (St. Louis, MO, USA). All chemicals were of analytical or reagent grade and were used without further purification.

HSA (from Sigma-Aldrich, St Louis, MO, USA) was essentially FA free and was used without further purification. The HSA stock solution ( $[HSA] = 1.2 \times 10^{-2}$  M) was prepared by dissolving HSA in  $2.0 \times 10^{-2}$  M Bis-tris propane buffer solution (pH 7.5). The HSA concentration was determined spectrophotometrically at 279 nm ( $\epsilon = 3.6 \times 10^4$  M $^{-1}$  cm $^{-1}$ ) [1]. Then, the HSA stock solution was diluted in the Bis-tris-propane buffer (0.1 M), at the desired pH; the final pH ranged between 5.8 and 9.5. The final HSA concentration ranged between  $2.0 \times 10^{-6}$  M and  $10 \times 10^{-4}$  M.

The NphOHe, NphODE, and NphOMy solutions were prepared by dissolving the substrates in a  $2.0 \times 10^{-2}$  M Bis-tris propane buffer solution (pH 7.5) in the presence of 10% acetonitrile. The NphOHe, NphODE, and NphOMy concentration was determined spectrophotometrically at 400 nm ( $\epsilon = 1.8 \times 10^4$  M $^{-1}$  cm $^{-1}$ ; pH > 8.5 and 22.0°C), allowing to calculate the amount of 4-nitrophenol released from the substrate [15]. The final NphOHe, NphODE, and NphOMy concentration ranged between  $2.0 \times 10^{-6}$  M and  $1.0 \times 10^{-4}$  M. The final acetonitrile concentration was 0.5% (v/v) [9,12,13].

Kinetics and thermodynamics of the HSA-Tyr411-catalyzed hydrolysis of NphOHe, NphODE, and NphOMy were followed spectrophotometrically at 405 nm by rapid mixing the HSA solution with the NphOHe, NphODE, and NphOMy solutions [9,12,13,15].

Kinetics and thermodynamics of the HSA-Tyr411-catalyzed hydrolysis of NphOHe, NphODE, and NphOMy, obtained under conditions where  $[NphOXx] \geq 5 \times [HSA]$  and  $[HSA] \geq 5 \times [NphOXx]$ , were analyzed in the framework of the minimum three step-mechanism reported in Fig. 1 [9,12–16].

Kinetics and thermodynamics of the HSA-Tyr411-catalyzed hydrolysis of NphOHe, NphODE, and NphOMy were also determined in the presence of diazepam, diflunisal, ibuprofen, 3-indoxyl-sulfate and propofol; the ligand concentration ranged between  $4.0 \times 10^{-6}$  M and  $8.0 \times 10^{-3}$  M.

Kinetic and thermodynamic parameters were obtained between pH 5.8 and 9.5, at 22.0°C.

Experiments were carried out with the SFM-200 rapid-mixing stopped-flow apparatus (Bio-Logic Science Instruments, Claix, France) and the Cary 50 Bio spectrophotometer (Varian Inc., Palo Alto, CA, USA).

Kinetics and thermodynamics of the HSA pseudo-esterase activity were analyzed using the GraphPad Prism program (GraphPad Software, Inc., La Jolla, CA, USA). The results are given as mean values of at least four experiments plus or minus the corresponding standard deviation.

## Results

### Pseudo-esterase activity of HSA-Tyr411

As previously reported for the HSA-Tyr411-catalyzed hydrolysis of NphOAc and NphOMy [12,13], the determination of kinetic parameters of Fig. 1 is simplified by the fact that the formation of the HSA:NphOHe and HSA:NphODE complexes can be treated as a rapid equilibrium process. Indeed, no lag phase occurs in the release of NphOH from NphOHe and NphODE in the presence of HSA (Fig. 2), indicating that the equilibration of HSA:NphOHe and HSA:NphODE with HSA and NphOHe and NphODE, respectively, is complete within 1.4 ms (*i.e.*,

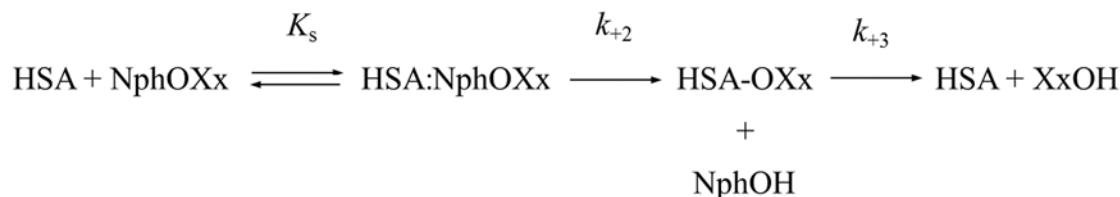


**Fig 1. The minimum three step-mechanism for the HSA-Tyr411-catalyzed hydrolysis of NphOHe, NphODE, and NphOMy.** HSA is the substrate-free protein, NphOXx is the substrate, HSA:NphOXx is the reversible protein-substrate complex, HSA-OXx is considered to be an ester formed between the acyl moiety of the substrate and the O atom of the Tyr411 phenoxyl group [14], XxOH is hexanoate or decanoate or myristate,  $K_s$  is the pre-equilibrium constant for the formation of the HSA:NphOXx complex,  $k_{+2}$  is the first-order acylation rate constant, and  $k_{+3}$  is the first-order deacylation rate constant. Xx indicates Ac or He or De or My.

doi:10.1371/journal.pone.0120603.g001

the “dead-time” of the rapid-mixing stopped-flow apparatus). Moreover, the rate of NphOH release from NphOHe and NphODE catalyzed by HSA-Tyr411 is unaffected by the addition of NphOH (up to  $1.0 \times 10^{-4}$  M) in the reaction mixtures (data not shown), indicating that the acylation step is essentially irreversible. If NphOH had affected the HSA-Tyr411 catalyzed hydrolysis of NphOHe and NphODE, the classical product (*i.e.*, NphOH) inhibition behavior would have been observed.

When  $[\text{HSA}] \geq 5 \times [\text{NphOHe}]$  and  $[\text{HSA}] \geq 5 \times [\text{NphODE}]$ , the reaction of HSA with NphOHe and NphODE displays a mono-exponential time-course (Fig. 2, panels A and B). Values of the pseudo-first order rate constant for the HSA-Tyr411-catalyzed hydrolysis of NphOHe and NphODE (*i.e.*, of NphOH release;  $k_{\text{app}}$ ) were obtained according to equation (1) [9,12,13]:

$$[\text{NphOXx}]_t = [\text{NphOXx}]_i \times (1 - e^{-k_{\text{app}} \times t}) \quad (1)$$

where Xx is De or He. Values of  $k_{\text{app}}$  were independent of the NphOHe and NphODE concentration under conditions where  $[\text{HSA}] \geq 5 \times [\text{NphOHe}]$  and  $[\text{HSA}] \geq 5 \times [\text{NphODE}]$ .

Values of  $K_s$  and  $k_{+2}$  for the HSA-Tyr411-catalyzed hydrolysis of NphOHe and NphODE (see Table 1) were obtained from the hyperbolic plots of  $k_{\text{app}}$  as a function of the HSA concentration (Fig. 2, panels C and D) according to equation (2) [9,12,13]:

$$k_{\text{app}} = (k_{+2} \times [\text{HSA}]) / (K_s + [\text{HSA}]) \quad (2)$$

When  $[\text{NphOHe}] \geq 5 \times [\text{HSA}]$  and  $[\text{NphODE}] \geq 5 \times [\text{HSA}]$ , the reaction of NphOHe and NphODE with HSA displays a mono-exponential time course (Fig. 2, panels E and F). Values of the pseudo-first-order rate constant for the HSA-Tyr411-catalyzed hydrolysis of NphOHe and NphODE (*i.e.*, of NphOH release;  $k_{\text{obs}}$ ) were obtained according to equation (3) [9,12,13]:

$$[\text{NphOXx}]_t = [\text{NphOXx}]_i \times (1 - e^{-k_{\text{obs}} \times t}) \quad (3)$$

Values of  $k_{\text{obs}}$  are independent of the HSA concentration when  $[\text{NphOHe}] \geq 5 \times [\text{HSA}]$  and  $[\text{NphODE}] \geq 5 \times [\text{HSA}]$ .

When  $k_{+2} \geq 5 \times k_{+3}$ , the differential equations arising from Fig. 1 may be solved [12,13,16,17] to describe the time course of NphOH release at the early stages of the reaction. The resulting expression is given in eqs (4)–(6) [12,13,16,17]:

$$[\text{NphOH}] = (\alpha \times [\text{HSA}] \times (1 - e^{-k_{\text{obs}} \times t})) + ((k_{\text{cat}} \times [\text{HSA}] \times [\text{NphOXx}] \times t) / (K_m + [\text{NphOXx}])) \quad (4)$$

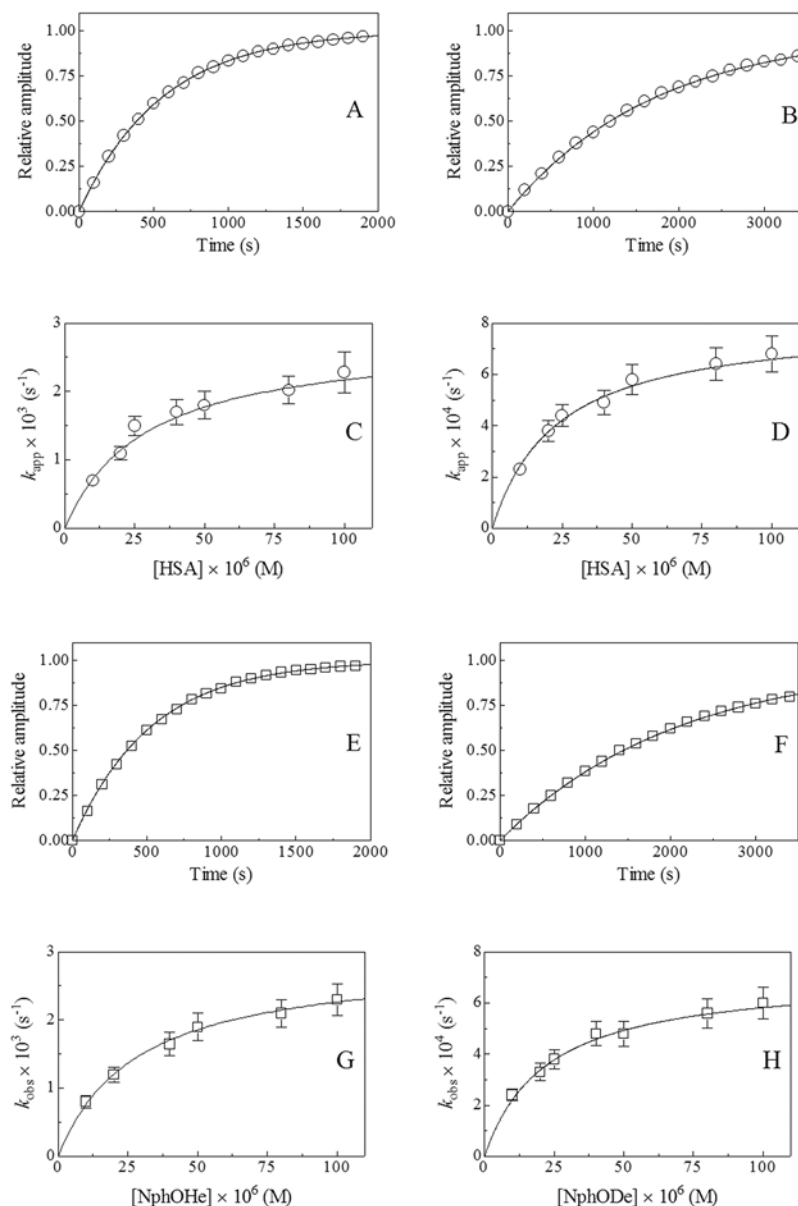


**Fig 2. HSA-mediated hydrolysis of NphOHe and NphODE.** Time course of the reaction of  $2.0 \times 10^{-6}$  M NphOHe (panel A) and NphODE (panel B) with  $5.0 \times 10^{-5}$  M HSA, i.e.  $[HSA] \geq 5 \times [NphOHe]$  and  $[HSA] \geq 5 \times [NphODE]$ , respectively. The continuous lines were calculated according [equation \(1\)](#) with  $k_{app} = (1.8 \pm 0.2) \times 10^{-3} \text{ s}^{-1}$  (panel A) and  $(5.8 \pm 0.6) \times 10^{-4} \text{ s}^{-1}$  (panel B). Dependence of  $k_{app}$  on the HSA concentration at  $[HSA] \geq 5 \times [NphOHe]$  (panel C) and  $[HSA] \geq 5 \times [NphODE]$  (panel D), respectively. The continuous lines were obtained according to [equation \(2\)](#) with the following parameters  $k_{+2} = (2.8 \pm 0.3) \times 10^{-3} \text{ s}^{-1}$  and  $K_s = (2.9 \pm 0.3) \times 10^{-5} \text{ M}$  (panel C), and  $k_{+2} = (8.1 \pm 0.8) \times 10^{-4} \text{ s}^{-1}$  and  $K_s = (2.3 \pm 0.3) \times 10^{-5} \text{ M}$  (panel D).  $[NphOHe]$  and  $[NphODE]$  was  $2.0 \times 10^{-6} \text{ M}$  and  $[HSA]$  ranged from  $1.0 \times 10^{-5} \text{ M}$  to  $1.0 \times 10^{-4} \text{ M}$ . Time course of the reaction of  $2.0 \times 10^{-6} \text{ M}$  HSA with  $5.0 \times 10^{-4} \text{ M}$  NphOHe (panel E) and NphODE (panel F), i.e.  $[NphOHe] \geq 5 \times [HSA]$  and  $[NphODE] \geq 5 \times [HSA]$ , respectively. The continuous lines were calculated according to [equation \(6\)](#) with  $k_{obs} = (1.9 \pm 0.2) \times 10^{-3} \text{ s}^{-1}$  (panel E) and  $(4.8 \pm 0.5) \times 10^{-4} \text{ s}^{-1}$  (panel F). Dependence of  $k_{obs}$  on the NphOHe and NphODE concentration at  $[NphOHe] \geq 5 \times [HSA]$  (panel G) and  $[NphODE] \geq 5 \times [HSA]$  (panel H). The continuous lines were obtained according to [equation \(6\)](#) with the following parameters  $k_{+2} = (2.9 \pm 0.3) \times 10^{-3} \text{ s}^{-1}$  and  $K_s = (2.8 \pm 0.3) \times 10^{-5} \text{ M}$  (panel G), and  $k_{+2} = (7.1 \pm 0.8) \times 10^{-4} \text{ s}^{-1}$  and  $K_s = (2.2 \pm 0.2) \times 10^{-5} \text{ M}$  (panel H). The value of  $k_{+3}$  approximates to  $0 \text{ s}^{-1}$ .  $[HSA]$  was  $2.0 \times 10^{-6} \text{ M}$ , and  $[NphOHe]$  and  $[NphODE]$  ranged from  $1.0 \times 10^{-5} \text{ M}$  to  $1.0 \times 10^{-4} \text{ M}$ . Where not shown, the standard deviation is smaller than the symbol. For details, see text.

doi:10.1371/journal.pone.0120603.g002

**Table 1. Values of catalytic parameters for the HSA-Tyr411-catalyzed hydrolysis of NphOHe, NphODE, and NphOMy, at pH 7.5 and 22.0°C.**

Substrate	[HSA] ≥ 5×[NphOXx]			[NphOXx] ≥ 5×[HSA]		
	$K_s$ (μM)	$k_{+2}$ (s <sup>-1</sup> )	$k_{+2}/K_s$ (M <sup>-1</sup> s <sup>-1</sup> )	$K_s$ (μM)	$k_{+2}$ (s <sup>-1</sup> )	$k_{+2}/K_s$ (M <sup>-1</sup> s <sup>-1</sup> )
NphOAc <sup>a</sup>	(4.8±0.5)×10 <sup>-4</sup>	(3.9±0.4)×10 <sup>-1</sup>	(8.1±0.9)×10 <sup>2</sup>	(4.7±0.5)×10 <sup>-4</sup>	(4.2±0.4)×10 <sup>-1</sup>	(8.4±0.9)×10 <sup>2</sup>
NphOHe <sup>b</sup>	(2.9±0.3)×10 <sup>-5</sup>	(2.8±0.3)×10 <sup>-3</sup>	(9.7±1.3)×10 <sup>1</sup>	(2.8±0.3)×10 <sup>-5</sup>	(2.9±0.3)×10 <sup>-3</sup>	(1.0±0.2)×10 <sup>2</sup>
NphODE <sup>b</sup>	(2.3±0.2)×10 <sup>-5</sup>	(8.1±0.8)×10 <sup>-4</sup>	(3.5±0.5)×10 <sup>1</sup>	(2.2±0.2)×10 <sup>-5</sup>	(7.1±0.8)×10 <sup>-4</sup>	(3.3±0.5)×10 <sup>1</sup>
NphOMy <sup>c</sup>	(2.6±0.3)×10 <sup>-5</sup>	(1.6±0.2)×10 <sup>-4</sup>	6.2±0.6	(2.5±0.3)×10 <sup>-5</sup>	(1.5±0.2)×10 <sup>-4</sup>	5.9±0.6

<sup>a</sup> From [13].

<sup>b</sup> Present study.

<sup>c</sup> From [12].

doi:10.1371/journal.pone.0120603.t001

where

$$\alpha = ((k_{+2} \times [\text{NphOXx}]) / ((k_{+2} + k_{+3}) \times (K_m + [\text{NphOXx}])))^2 \quad (5)$$

and

$$k_{\text{obs}} = ((k_{+2} \times [\text{NphOXx}]) / (K_s + [\text{NphOXx}])) + k_{+3} \quad (6)$$

As predicted from eqs (4)–(6), a “burst” phase of NphOH release of amplitude  $\alpha$  with the first order rate constant  $k_{\text{obs}}$  occurs. Values of  $\alpha$ , obtained at [NphOHe] ≥ 5×[HSA] and [NphODE] ≥ 5×[HSA], range between 0.99 and 1.03 (S1 Table), indicating that the HSA: NphOXx:NphOH stoichiometry is 1:1:1. Moreover, the time course of the “burst” phase of NphOH release is a first-order process for more than 95% of its course (Fig. 2, panels E and F) as estimated from residual analysis. Values of  $k_{\text{obs}}$  are independent of the HSA concentration when [NphOHe] ≥ 5×[HSA] and [NphODE] ≥ 5×[HSA]. Values of  $K_s$  and  $k_{+2}$  (see Table 1) were determined from hyperbolic plots of  $k_{\text{obs}}$  versus [NphOXx] (Fig. 2, panels G and H) according to equation (6) [16,17]. Under all the experimental conditions, the y-intercept of the hyperbola described by equation (6) was  $< 2 \times 10^{-6} \text{ s}^{-1}$ , thus indicating that the value of  $k_{+3}$  is at least 100-fold smaller than that of  $k_{\text{obs}}$  obtained at the lowest NphOHe and NphODE concentration (i.e.,  $k_{+3} < 2 \times 10^{-6} \text{ s}^{-1}$ ).

As predicted from Fig. 1, values of  $K_s$  and  $k_{+2}$  obtained under conditions where [HSA] ≥ 5×[NphOHe] and [HSA] ≥ 5×[NphODE] from equation (2) are in excellent agreement with those obtained under conditions where [NphOHe] ≥ 5×[HSA] and [NphODE] ≥ 5×[HSA] from equation (6) (Table 1). Moreover, data here reported indicate that the deacylation process is rate limiting in the HSA-Tyr411-catalyzed hydrolysis of NphOHe and NphODE, as previously reported for NphOAc and NphOMy [12,13] (i.e.,  $k_{+3} \ll k_{+2}$ ). Furthermore, values of  $K_s$  and  $k_{+2}$  here obtained for the HSA-Tyr411-catalyzed hydrolysis of NphOHe and NphODE agree with those previously reported [9].

## pH effects on the pseudo-esterase activity of HSA-Tyr411

Values of catalytic parameters for the HSA-Tyr411-catalyzed hydrolysis of NphOHe and NphODE obtained between pH 5.8 and 9.5 (at 22.0°C) are summarized in S2 and S3 Tables. Fig. 3 shows the pH dependence of  $K_s$ ,  $k_{+2}$ , and  $k_{+2}/K_s$  values for the HSA-Tyr411-catalyzed



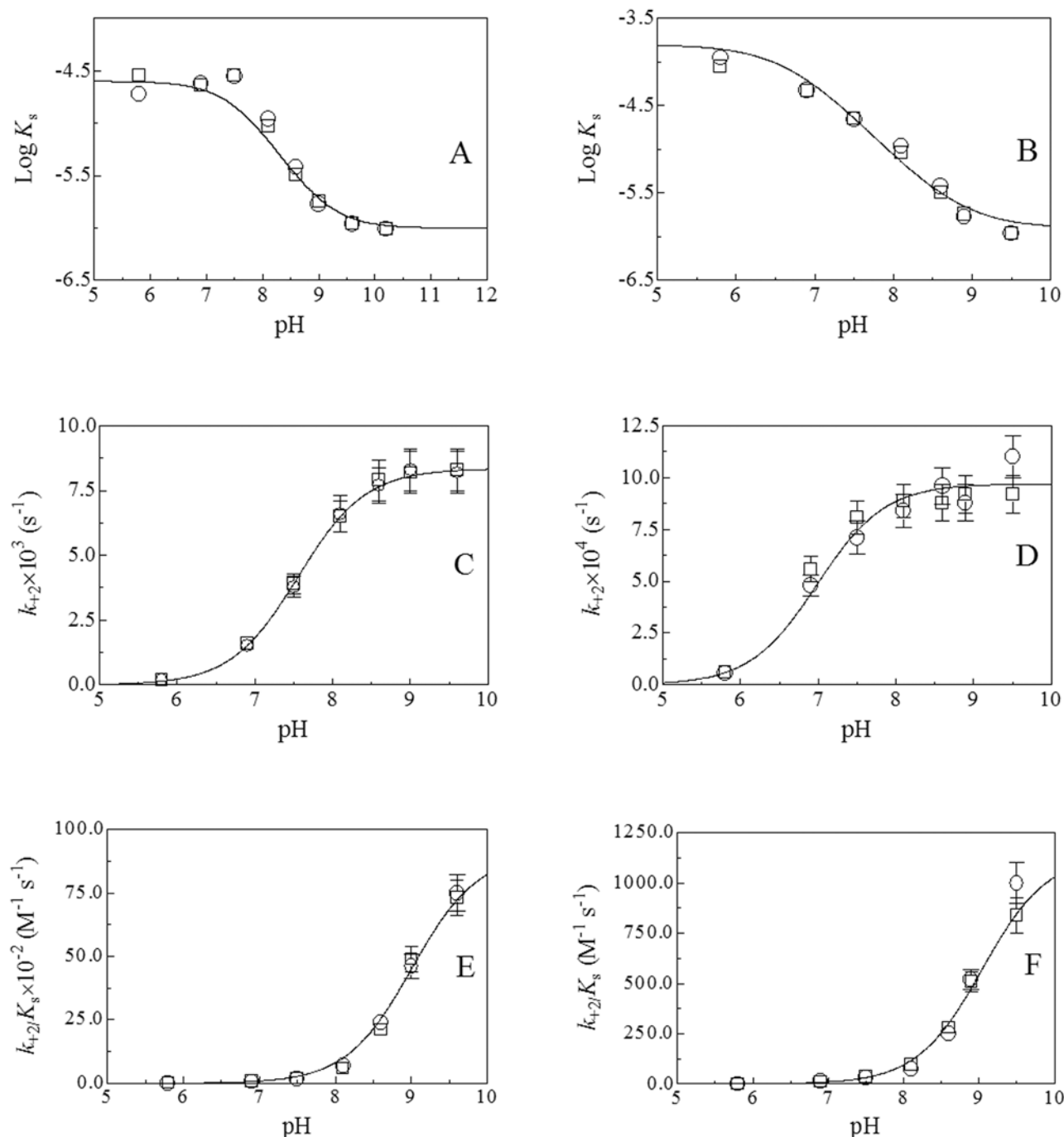


**Fig 3. pH dependence of Log  $K_s$  (panels A and B),  $k_{+2}$  (panels C and D), and  $k_{+2}/K_s$  (panels E and F) for HSA-mediated hydrolysis of NphOHe (panels A, C, and E) and NphODe (panels B, D, and F), at 22.0°C.** Circles indicate data obtained under conditions where [HSA] ≥ 5 × [NphOHe] and [HSA] ≥ 5 × [NphODe]. Squares indicate data obtained under conditions where [NphOHe] ≥ 5 × [HSA] and [NphODe] ≥ 5 × [HSA]. The continuous lines in panels A and B, C and D, and E and F were obtained from data analysis according to eqs (7)–(9), respectively, with values of parameters given in Table 2. Where not shown, the standard deviation is smaller than the symbol. For details, see text.

doi:10.1371/journal.pone.0120603.g003

**Table 2.  $pK_{\text{unl}}$  and  $pK_{\text{lig}}$  values as well as of alkaline limiting values of  $k_{+2}$ ,  $K_s$ , and  $k_{+2}/K_s$  for the HSA-Tyr411-catalyzed hydrolysis of NphOAc; NphOHe, NphODE, and NphOMy, at 22.0°C.**

NphOFA	$K_s$	$K_s^{\text{lim}}$ (M)	$k_{+2}$	$k_{+2}^{\text{lim}}$ ( $\text{s}^{-1}$ )	$k_{+2}/K_s$	$(k_{+2}/K_s)^{\text{lim}}$ ( $\text{M}^{-1} \text{s}^{-1}$ )
NphOAc <sup>a</sup>	$pK_{\text{unl}} = 9.0 \pm 0.1$	$(6.6 \pm 0.7) \times 10^{-5}$			$pK_{\text{unl}} = 9.0 \pm 0.1$	$(3.4 \pm 0.4) \times 10^4$
	$pK_{\text{lig}} = 8.1 \pm 0.2$		$pK_{\text{lig}} = 8.1 \pm 0.2$	$2.1 \pm 0.2$		
NphOHe <sup>b</sup>	$pK_{\text{unl}} = 8.9 \pm 0.2$	$(9.8 \pm 1.0) \times 10^{-7}$			$pK_{\text{unl}} = 9.0 \pm 0.1$	$(9.1 \pm 1.0) \times 10^3$
	$pK_{\text{lig}} = 7.5 \pm 0.2$		$pK_{\text{lig}} = 7.6 \pm 0.2$	$(8.3 \pm 0.8) \times 10^{-3}$		
NphODE <sup>b</sup>	$pK_{\text{unl}} = 8.9 \pm 0.1$	$(1.3 \pm 0.1) \times 10^{-6}$			$pK_{\text{unl}} = 8.9 \pm 0.2$	$(9.6 \pm 1.1) \times 10^2$
	$pK_{\text{lig}} = 6.9 \pm 0.2$		$pK_{\text{lig}} = 7.0 \pm 0.2$	$(9.8 \pm 1.1) \times 10^{-4}$		
NphOMy <sup>c</sup>	$pK_{\text{unl}} = 8.8 \pm 0.1$	$(1.4 \pm 0.1) \times 10^{-6}$			$pK_{\text{unl}} = 8.9 \pm 0.1$	$(2.2 \pm 0.2) \times 10^2$
	$pK_{\text{lig}} = 6.7 \pm 0.2$		$pK_{\text{lig}} = 6.9 \pm 0.2$	$(2.3 \pm 0.2) \times 10^{-4}$		

<sup>a</sup> From [13].

<sup>b</sup> Present study.

<sup>c</sup> From [12].

doi:10.1371/journal.pone.0120603.t002

hydrolysis of NphOHe and NphODE. Values of  $pK_a$  modulating the pH dependence of  $k_{+2}/K_s$ ,  $k_{+2}$ , and  $K_s$  were determined by data analysis according to eqs (7)–(9) [9,12,13,15–17]:

$$\text{Log}K_s = -\text{Log}K_s^{\text{lim}} + \text{Log}((10^{-\text{pH}} + 10^{-pK_{\text{unl}}})/(10^{-\text{pH}} + 10^{-pK_{\text{lig}}})) \quad (7)$$

$$k_{+2} = k_{+2}^{\text{lim}}/(1 + (10^{-\text{pH}}/10^{-pK_{\text{lig}}})) \quad (8)$$

$$k_{+2}/K_s = (k_{+2}/K_s)^{\text{lim}}/(1 + (10^{-\text{pH}}/10^{-pK_{\text{unl}}})) \quad (9)$$

where  $K_s^{\text{lim}}$ ,  $k_{+2}^{\text{lim}}$ , and  $(k_{+2}/K_s)^{\text{lim}}$  are the values corresponding to the alkaline asymptotes of  $K_s$ ,  $k_{+2}$ , and  $k_{+2}/K_s$ .

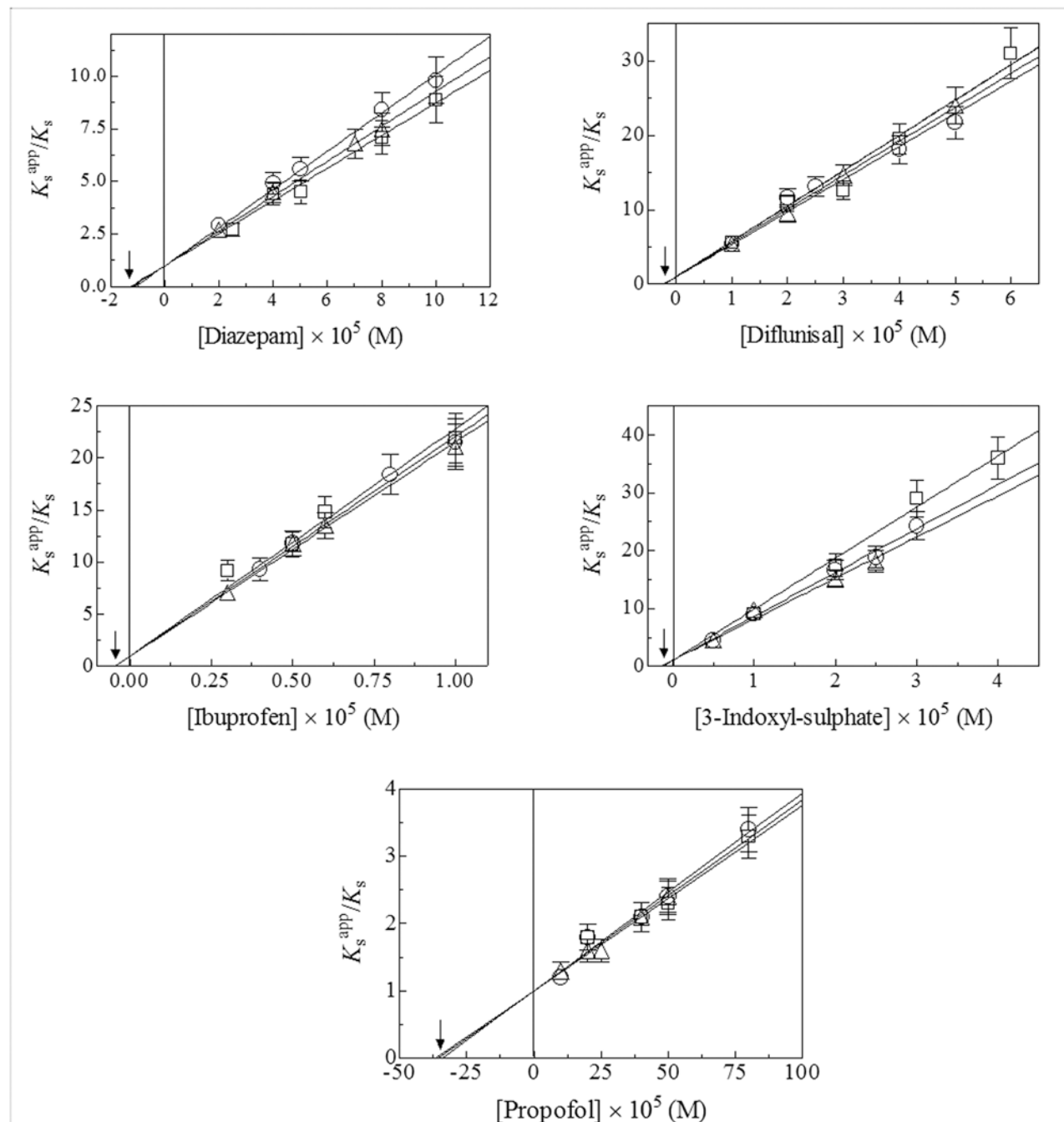
According to linked functions [12,13,16–18], the pH dependence of  $K_s$  reflects the acidic  $pK_a$ -shift of a single amino acid residue from free HSA (*i.e.*,  $pK_{\text{unl}}$ ) to the HSA:NphOHe and HSA:NphODE complexes (*i.e.*,  $pK_{\text{lig}}$ ). Moreover, the pH dependence of  $k_{+2}$  and  $k_{+2}/K_s$  reflects the acid-base equilibrium of one apparent ionizing group in the HSA:NphOHe and HSA:NphODE complexes (*i.e.*,  $pK_{\text{lig}}$ ) and in free HSA (*i.e.*,  $pK_{\text{unl}}$ ), respectively. As expected [12,13,16–18], the  $pK_a$  value of free HSA (*i.e.*,  $pK_{\text{unl}}$ ) is independent of the substrate whereas the  $pK_a$  values of the HSA:NphOHe and HSA:NphODE complexes (*i.e.*,  $pK_{\text{lig}}$ ) depend on the substrate (Table 2).

## Competitive inhibition of the pseudo-esterase activity of HSA-Tyr411

As shown in Fig. 4, diazepam, diflunisal, ibuprofen, 3-indoxyl-sulfate, and propofol inhibit the Tyr411-catalyzed hydrolysis of NphOHe, NphODE, and NphOMy. As expected for the pure competitive inhibition mechanism [19], values of  $K_s$  for the HSA-Tyr411-catalyzed hydrolysis of NphOHe, NphODE, and NphOMy (Fig. 4) increase with the diazepam, diflunisal, ibuprofen, 3-indoxyl-sulfate, and propofol concentration whereas values of  $k_{+2}$  are unaffected by the ligand concentration (S1, S2, and S3 Figs.). The analysis of the linear dependence of the  $K_s^{\text{app}}/K_s$  ratio on the ligand concentration (*i.e.*, [ligand]) according to equation (10) [19]:

$$K_s^{\text{app}}/K_s = ([\text{ligand}]/K_i) + 1 \quad (10)$$



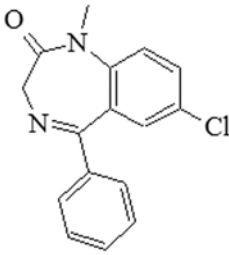
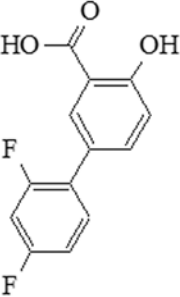
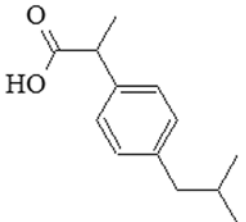
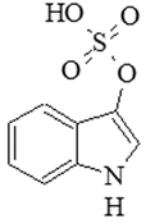
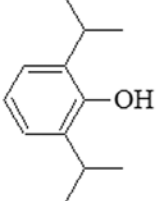


**Fig 4. Competitive inhibitory effect of diazepam, diflunisal, ibuprofen, 3-indoxyl-sulfate, and propofol on the HSA-Tyr411-catalyzed hydrolysis of NphOHe (squares), NphODE (circles), and NphOMy (triangles).** Data were obtained under conditions where  $[NphOHe] > 5 \times [HSA]$ . The analysis of data according to [equation \(10\)](#) allowed to determine values of  $K_i$  (indicated by arrows) reported in [Fig. 5](#). Where not shown, the standard deviation is smaller than the symbol. For details, see text.

doi:10.1371/journal.pone.0120603.g004

allowed to determine the values of the equilibrium dissociation constant for diazepam, diflunisal, ibuprofen, 3-indoxyl-sulfate, and propofol binding to the FA3-FA4 cleft of HSA (*i.e.*,  $K_i$ , corresponding to the absolute value of the  $x$  intercept of the linear plot). As expected for the pure competitive inhibition mechanism [19], values of  $K_i$  for diazepam, diflunisal, ibuprofen,

3-indoxyl-sulfate, and/or propofol binding to the FA3-FA4 cleft of HSA are independent of NphOAc [13], NphOHe (present study), NphODE (present study), and NphOMy (see [12] and present study) (Fig. 5). Values of  $K_i$  for diazepam, diflunisal, ibuprofen, 3-indoxyl-sulfate, and propofol binding to HSA here obtained (Fig. 5) agree with those reported previously [2,12,13,20–26].

Ligand	Structure	4-nitrophenyl ester	$K_i$ (M)
Diazepam		NphOAc <sup>a</sup>	$1.2 \times 10^{-5}$
		NphOHe <sup>b</sup>	$(1.3 \pm 0.2) \times 10^{-5}$
		NphODE <sup>b</sup>	$(1.1 \pm 0.2) \times 10^{-5}$
		NphOMy <sup>b</sup>	$(1.2 \pm 0.3) \times 10^{-5}$
		NphOMy <sup>c</sup>	$1.0 \times 10^{-5}$
Diflunisal		NphOHe <sup>b</sup>	$(2.1 \pm 0.2) \times 10^{-6}$
		NphODE <sup>b</sup>	$(2.3 \pm 0.3) \times 10^{-6}$
		NphOMy <sup>b</sup>	$(2.2 \pm 0.3) \times 10^{-6}$
Ibuprofen		NphOHe <sup>b</sup>	$(4.6 \pm 0.6) \times 10^{-7}$
		NphODE <sup>b</sup>	$(4.8 \pm 0.5) \times 10^{-7}$
		NphOMy <sup>b</sup>	$(4.9 \pm 0.6) \times 10^{-7}$
3-Indoxyl-sulfate		NphOHe <sup>b</sup>	$(1.1 \pm 0.2) \times 10^{-6}$
		NphODE <sup>b</sup>	$(1.3 \pm 0.2) \times 10^{-6}$
		NphOMy <sup>b</sup>	$(1.4 \pm 0.2) \times 10^{-6}$
Propofol		NphOHe <sup>b</sup>	$(3.5 \pm 0.4) \times 10^{-4}$
		NphODE <sup>b</sup>	$(3.4 \pm 0.4) \times 10^{-4}$
		NphOMy <sup>b</sup>	$(3.6 \pm 0.4) \times 10^{-4}$

**Fig 5. Values of  $K_i$  for the competitive inhibition of the HSA-Tyr411-catalyzed hydrolysis of NphOAc, NphOHe, NphODE, and NphOMy by diazepam, diflunisal, ibuprofen, 3-indoxyl-sulfate, and/or propofol, at pH 7.5 and 22.0°C.** <sup>a</sup> From [13]. <sup>b</sup> Present study. <sup>c</sup> From [12].

doi:10.1371/journal.pone.0120603.g005

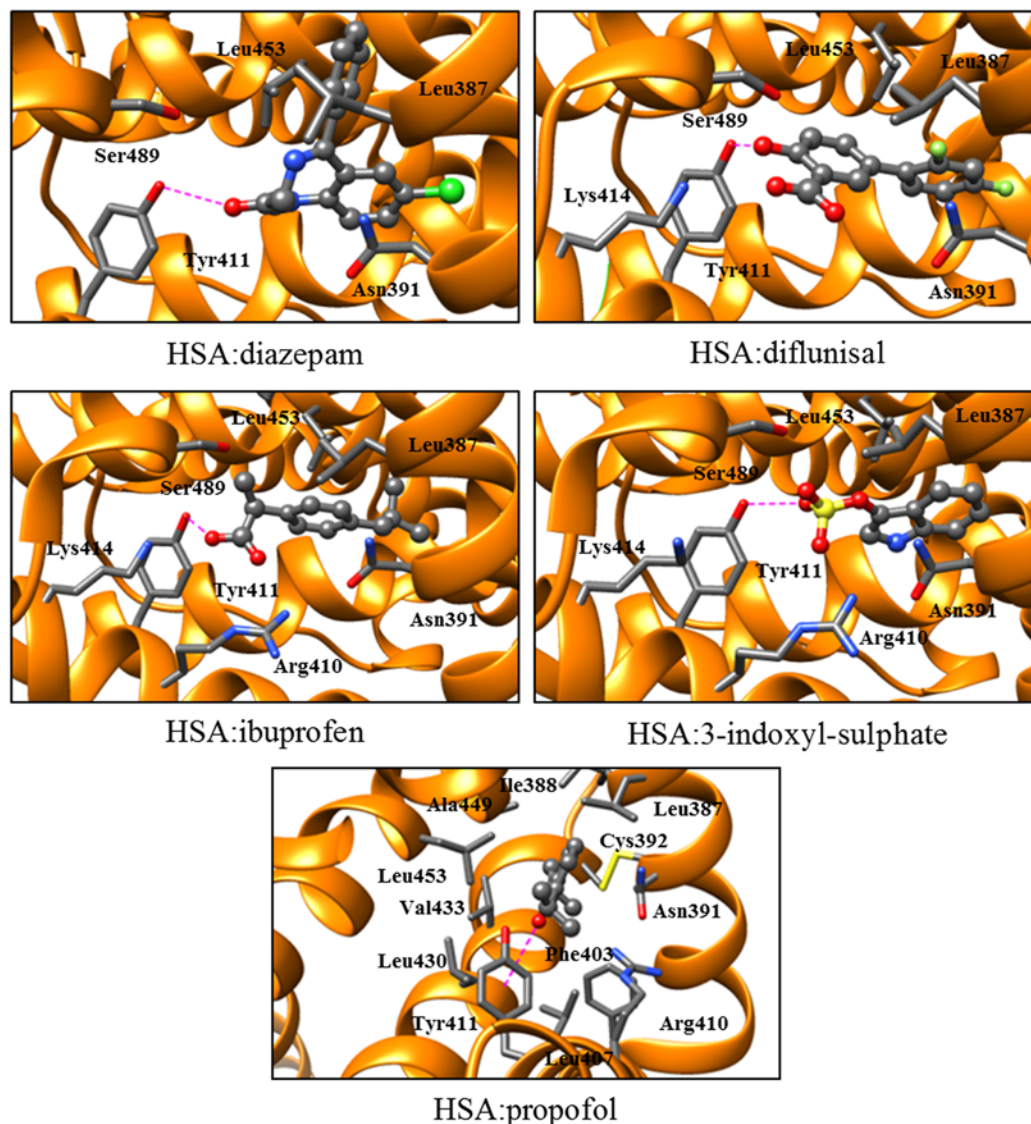


**Fig 6. Three-dimensional structures of the HSA: diazepam, : diflunisal, : ibuprofen, : 3-indoxyl-sulfate, and : propofol complexes.** The ligands are shown in the ball-and-stick representation. The Tyr411 phenoxyl O atom of HSA is hydrogen bond to a O atom of diazepam, diflunisal, ibuprofen, and 3-indoxyl-sulfate. The Leu430 carbonyl O atom of HSA is hydrogen bond to the O atom of propofol. The hydrogen bonds are represented as red dashed lines. The PDB ID codes of HSA: diazepam, : diflunisal, : ibuprofen, : 3-indoxyl-sulfate, and : propofol complexes are 2BXE, 2BXF, 2BXG, 2BXH, and 1E7A, respectively [8,30]. The pictures were drawn with the UCSF-Chimera package [46]. For details, see text.

doi:10.1371/journal.pone.0120603.g006

## Discussion

The hydrolysis of NphOAc, NphOHe, NphODE, and NphOMy by HSA-Tyr411 (see [12–15] and present study) is reminiscent of that observed for acylating agents with proteases [27]. In fact, NphOAc [13], NphOHe (present study), NphODE (present study), and NphOMy [12] act as suicide substrates of HSA-Tyr411, values of the deacylation rate constant for all four substrates (*i.e.*,  $k_{+3}$ ) being lower by several orders of magnitude than those of the acylation rate constant (*i.e.*,  $k_{+2}$ ). Remarkably, HSA acylation appears to modulate ligand binding. In fact, HSA acylation by aspirin [28] increases the affinity of phenylbutazone and inhibits bilirubin

and prostaglandin binding, thus accelerating the clearance of prostaglandins, which represents an additional mechanism of the aspirin anti-inflammatory action [29].

Kinetics for the hydrolysis of NphOHe and NphODE by HSA are pH dependent, reflecting the acidic  $pK_a$  shift of an apparently single ionizing group of HSA upon substrate binding. This could reflect the reduced solvent accessibility of the Tyr411 residue, representing the primary esterase site of HSA (see [9,12–14]), although long range effects could not be ruled out. The Tyr411 catalytic residue is located in the FA3-FA4 cleft, which is made by an apolar region forming the FA3 site and a polar patch contributing the FA4 site. The polar patch is centered on the Tyr411 side chain and includes Arg410, Lys414, and Ser489 residues [8,30,31]. The inspection of the three-dimensional structure of the ligand-free HSA [32] and of the molecular model of the HSA:4-nitrophenyl propionate complex [9] suggests that the observed pH effects (Fig. 3) could reflect the acidic  $pK_a$  shift of the Tyr411 residue upon substrate binding. This would render more stable the negative charge on the phenoxyl O atom of Tyr411, which appears to be hydrogen bonded to the carbonyl O atom of 4-nitrophenyl propionate [9], potentiating its nucleophilic role as an electron donor in the pseudo-esterase activity of HSA. Of note, the acidic shift of the  $pK_a$  value of the ionizing group affecting catalysis from  $8.9 \pm 0.1$  in ligand free-HSA to  $8.1 \pm 0.2$ ,  $7.6 \pm 0.2$ ,  $7.0 \pm 0.2$ , and  $6.8 \pm 0.2$  in the HSA:NphOAc, HSA:NphOHe, HSA:NphODE, and HSA:NphOMy complexes (see Table 2), respectively, depends on the length of the fatty acid tail. Therefore, it appears as the increase of the FA tail length brings about the progressive reduction of the water solvent accessibility, thus enhancing the hydrophobicity of the catalytic site and leading to a decreased  $pK_a$  of the ionizing group modulating the catalysis. Of note, the pH dependence of the Tyr411-associated esterase activity parallels the pH-dependent neutral-to-basic allosteric transition of HSA [3].

Diazepam, diflunisal, ibuprofen, 3-indoxyl-sulfate, and/or propofol inhibit competitively the hydrolysis of NphOAc [13], NphOHe (present study), NphODE (present study), and NphOMy (see [12] and present study) (Fig. 5) by impairing the accessibility of 4-nitrophenyl esters to the Tyr411 catalytic center. In particular, diazepam, diflunisal, ibuprofen, and 3-indoxyl-sulfate bind to the center of the FA3-FA4 cleft, with one O atom being hydrogen bonded to the Tyr411 OH group (Fig. 6). On the other hand, propofol binds to the apolar region of the FA3-FA4 cleft with the phenolic OH group making a hydrogen bond with the carbonyl O atom of Leu430. Moreover, the aromatic ring of the propofol is sandwiched between the Asn391 and Leu453 side chains. Furthermore, one of the two isopropyl groups of propofol makes several apolar contacts at one end of the pocket, whereas the other is solvent exposed at the cleft entrance making close contacts with Asn391, Leu407, Arg410, and Tyr411 (Fig. 6) [8,30,31].

The different  $K_I$  values for diazepam, diflunisal, ibuprofen, 3-indoxyl-sulfate, and propofol binding to HSA (Fig. 5) agree with the selectivity of the FA3-FA4 cleft of HSA, which can be ascribed to the presence of a basic polar patch located at one end of the apolar FA3-FA4 cleft. Remarkably, diazepam, diflunisal, ibuprofen, and 3-indoxyl-sulfate are oriented with at least one O atom in the vicinity of the polar patch. On the other hand, the single polar hydroxyl group in the center of propofol does not interact with the polar patch of the FA3-FA4 cleft. Moreover, the FA3-FA4 cleft appears to adopt different ligand-dependent shapes, thus paying different free energy contributions for structural rearrangements [8].

## Conclusion

Due to the relevant physiological role of HSA in human plasma, *in vivo* implications can be argued from the present results. Accounting for the plasma levels of HSA (*i.e.*,  $[HSA] = 7.5 \times 10^{-4}$  M) [2] as well as of diflunisal, ibuprofen, and 3-indoxyl-sulfate plasma levels (*i.e.*, [ligand]; see

below) and  $K_I$  values for ligand binding (Fig. 4 and Fig. 5), the molar fraction (*i.e.*,  $Y$ ) of diazepam, diflunisal, ibuprofen, 3-indoxyl-sulfate, and propofol bound to plasmatic HSA was calculated according to equation (11) [33]:

$$[HSA] \times Y^2 - ([\text{ligand}] + [HSA] + K_I) \times Y + [\text{ligand}] = 0 \quad (11)$$

The following therapeutic plasma levels of the drugs investigated are commonly reported at steady-state: (i) 0.3–0.4  $\mu\text{g/mL}$  (*i.e.*,  $1.1 \times 10^{-6}$  M to  $1.1 \times 10^{-6}$  M) of diazepam are recommended for anxiolytic effects, and *ca.* 0.6  $\mu\text{g/mL}$  (*i.e.*,  $2.1 \times 10^{-6}$  M) for control of seizures; higher concentrations might suggest misuse or abuse [34–36]; (ii) 90–110  $\mu\text{g/mL}$  (*i.e.*,  $3.6 \times 10^{-4}$  M to  $5.3 \times 10^{-4}$  M) of diflunisal are usually required for anti-inflammatory effects [37,38]; (iii) 20–40  $\mu\text{g/mL}$  (*i.e.*,  $9.7 \times 10^{-5}$  M to  $1.9 \times 10^{-4}$  M) are observed after a single oral anti-inflammatory dose of ibuprofen [39,40]; and (iv) 1–2  $\mu\text{g/mL}$  (*i.e.*,  $5.6 \times 10^{-6}$  M to  $1.1 \times 10^{-5}$  M) of propofol are necessary to maintain sleep [41,42]. Conversely, 3-indoxyl-sulfate is an uremic toxin accumulated in the plasma of chronic kidney disease patients and induces an oxidative stress in a variety of cells such as renal tubular cells, glomerular mesangial cells, vascular smooth muscle cells, vascular endothelial cells, and osteoblasts. Under pathological conditions, the plasma concentration of 3-indoxyl-sulfate ranges between 4 and 60  $\mu\text{g/mL}$  (*i.e.*,  $1.9 \times 10^{-5}$  M to  $2.8 \times 10^{-4}$  M) [43,44].

Since the plasma levels of diflunisal, ibuprofen, and 3-indoxyl-sulfate (see above) are higher than values of  $K_I$  for ligand binding to HSA by about 100 folds (see Fig. 4 and Fig. 5), the molar fraction of diflunisal, ibuprofen, and 3-indoxyl-sulfate bound to HSA is higher than 0.9, according to equation (11). Although the commonly reported diazepam and propofol plasma levels (see above) are lower than the corresponding values of  $K_I$  for drug binding to HSA (see Fig. 4 and Fig. 5) by about 5 and 100 folds, respectively, the plasma HSA concentration (see above) is higher than  $K_I$  for by about 70 and 2 folds, respectively. According to equation (11), the molar fraction of diazepam and propofol bound to HSA in plasma is higher than 0.9 and 0.5, respectively.

As a whole, data here reported highlight the role of drugs diazepam, diflunisal, ibuprofen, and propofol as well as of the uremic toxin 3-indoxyl-sulfate to inhibit competitively the pseudo-esterase activity of HSA, Tyr411 representing the nucleophile. This aspect is appropriate since HSA acylation appears to modulate ligand binding [28,29] and the detoxification of several compounds [2,3]. Last, HSA not only acts as a carrier and as a detoxifier but also displays transient drug- and toxin-based properties, representing a case for “chronosteric effects” [45]. This opens the scenario toward the possibility of a drug- and toxin-dependent multiplicity of roles for HSA.

## Supporting Information

**S1 Fig. Effect of diazepam, diflunisal, ibuprofen, 3-indoxyl-sulphate, and propofol on the  $k_{+2}$  value for the HSA-Tyr411-catalyzed hydrolysis of NphOHe, at pH 7.5 and 22.0°C.** The filled square on the ordinate indicates the  $k_{+2}$  value obtained in the absence of the ligands. (DOC)

**S2 Fig. Effect of diazepam, diflunisal, ibuprofen, 3-indoxyl-sulphate, and propofol on the  $k_{+2}$  value for the HSA-Tyr411-catalyzed hydrolysis of NphODE, at pH 7.5 and 22.0°C.** The filled square on the ordinate indicates the  $k_{+2}$  value obtained in the absence of the ligands. (DOCX)

**S3 Fig. Effect of diazepam, diflunisal, ibuprofen, 3-indoxyl-sulphate, and propofol on the  $k_{+2}$  value for the HSA-Tyr411-catalyzed hydrolysis of NphOMy, at pH 7.5 and 22.0°C.** The filled square on the ordinate indicates the  $k_{+2}$  value obtained in the absence of the ligands. (DOCX)



**S1 Table. Values of  $\alpha$  for the HSA-Tyr411-catalyzed hydrolysis of NphOHe and NphODE, at 22.0°C.**

(DOC)

**S2 Table. Values of catalytic parameters for the HSA-Tyr411-catalyzed hydrolysis of NphOHe, at 22.0°C.**

(DOCX)

**S3 Table. Values of catalytic parameters for the HSA-Tyr411-catalyzed hydrolysis of NphODE, at 22.0°C.**

(DOC)

## Author Contributions

Conceived and designed the experiments: PA VT MC MF. Performed the experiments: LL MG ADM. Analyzed the data: LL GF MG ADM. Contributed reagents/materials/analysis tools: PA. Wrote the paper: PA VT MF.

## References

1. Peters T Jr. All about Albumin: Biochemistry, Genetics and Medical Applications. San Diego and London, Academic Press; 1996. doi: [10.1021/jp076583h](https://doi.org/10.1021/jp076583h) PMID: [18229913](https://pubmed.ncbi.nlm.nih.gov/18229913/)
2. Fanali G, di Masi A, Trezza V, Marino M, Fasano M, Ascenzi P. Human serum albumin: from bench to bedside. *Mol Aspects Med.* 2012; 33: 209–290. doi: [10.1016/j.mam.2011.12.002](https://doi.org/10.1016/j.mam.2011.12.002) PMID: [22230555](https://pubmed.ncbi.nlm.nih.gov/22230555/)
3. Kragh-Hansen U. Molecular and practical aspects of the enzymatic properties of human serum albumin and of albumin-ligand complexes. *Biochim Biophys Acta.* 2013; 1830: 5535–5544. doi: [10.1016/j.bbagen.2013.03.015](https://doi.org/10.1016/j.bbagen.2013.03.015) PMID: [23528895](https://pubmed.ncbi.nlm.nih.gov/23528895/)
4. Walker JE. Lysine residue 199 of human serum albumin is modified by acetylsalicylic acid. *FEBS Lett.* 1976; 66: 173–175. PMID: [955075](https://pubmed.ncbi.nlm.nih.gov/955075/)
5. Watanabe H, Tanase S, Nakajou K, Maruyama T, Kragh-Hansen U, Otagiri M. Role of Arg-410 and Tyr-411 in human serum albumin for ligand binding and esterase-like activity. *Biochem J.* 2000; 349: 813–819. PMID: [10903143](https://pubmed.ncbi.nlm.nih.gov/10903143/)
6. Díaz N, Suárez D, Sordo TL, Merz KM Jr. Molecular dynamics study of the IIA binding site in human serum albumin: influence of the protonation state of Lys195 and Lys199. *J Med Chem.* 2001; 44: 250–260. PMID: [11170635](https://pubmed.ncbi.nlm.nih.gov/11170635/)
7. Kragh-Hansen U, Chuang VT, Otagiri M. Practical aspects of the ligand-binding and enzymatic properties of human serum albumin. *Biol Pharm Bull.* 2002; 25: 695–704. PMID: [12081132](https://pubmed.ncbi.nlm.nih.gov/12081132/)
8. Ghuman J, Zunszain PA, Petitpas I, Bhattacharya AA, Otagiri M, Curry S. Structural basis of the drug-binding specificity of human serum albumin. *J Mol Biol.* 2005; 353: 38–52. PMID: [16169013](https://pubmed.ncbi.nlm.nih.gov/16169013/)
9. Sakurai Y, Ma SF, Watanabe H, Yamaotsu N, Hirono S, Kurono Y, et al. Esterase-like activity of serum albumin: characterization of its structural chemistry using p-nitrophenyl esters as substrates. *Pharm Res.* 2004; 21: 285–292. PMID: [15032310](https://pubmed.ncbi.nlm.nih.gov/15032310/)
10. Ohta N, Kurono Y, Ikeda K. Esterase-like activity of human serum albumin II: reaction with N-trans-cinnamoylimidazoles. *J Pharm Sci.* 1983; 72: 385–388. PMID: [6864475](https://pubmed.ncbi.nlm.nih.gov/6864475/)
11. Kurono Y, Kushida I, Tanaka H, Ikeda K. Esterase-like activity of human serum albumin. VIII. Reaction with amino acid p-nitrophenyl esters. *Chem Pharm Bull.* 1992; 40: 2169–2172. PMID: [1423775](https://pubmed.ncbi.nlm.nih.gov/1423775/)
12. Ascenzi P, Fasano M. Pseudo-enzymatic hydrolysis of 4-nitrophenyl myristate by human serum albumin. *Biochem Biophys Res Commun.* 2012; 422: 219–223. doi: [10.1016/j.bbrc.2012.04.111](https://doi.org/10.1016/j.bbrc.2012.04.111) PMID: [22560903](https://pubmed.ncbi.nlm.nih.gov/22560903/)
13. Ascenzi P, Gioia M, Fanali G, Coletta M, Fasano M. Pseudo-enzymatic hydrolysis of 4-nitrophenyl acetate by human serum albumin: pH-dependence of rates of individual steps. *Biochem Biophys Res Commun.* 2012; 424: 451–455. doi: [10.1016/j.bbrc.2012.06.131](https://doi.org/10.1016/j.bbrc.2012.06.131) PMID: [22771811](https://pubmed.ncbi.nlm.nih.gov/22771811/)
14. Lockridge O, Xue W, Gaydess A, Grigoryan H, Ding SJ, Schopfer LM, et al. Pseudo-esterase activity of human albumin: slow turnover on tyrosine 411 and stable acetylation of 82 residues including 59 lysines. *J Biol Chem.* 2008; 283: 22582–22590. doi: [10.1074/jbc.M802555200](https://doi.org/10.1074/jbc.M802555200) PMID: [18577514](https://pubmed.ncbi.nlm.nih.gov/18577514/)
15. Means GE, Bender ML. Acetylation of human serum albumin by p-nitrophenyl acetate. *Biochemistry.* 1975; 14: 4989–4994. PMID: [241394](https://pubmed.ncbi.nlm.nih.gov/241394/)



16. Hollaway MR, Antonini E, Brunori M. The pH-dependence of rates of individual steps in ficin catalysis. *Eur J Biochem.* 1971; 24: 332–341. PMID: [5157300](#)
17. Antonini E, Ascenzi P. The mechanism of trypsin catalysis at low pH: proposal for a structural model. *J Biol Chem.* 1981; 256: 12449–12455. PMID: [7298667](#)
18. Peller L, Alberty RA. Multiple intermediates in steady state enzyme kinetics. I. The mechanism involving a single substrate and product. *J Am Chem Soc.* 1959; 81: 5907–5914.
19. Ascenzi P, Ascenzi MG, Amiconi G. Enzyme competitive inhibition. Graphical determination of  $K_i$  and presentation of data in comparative studies. *Biochem Mol Biol Edu.* 1987; 15: 134–135.
20. Kragh-Hansen U. Molecular aspects of ligand binding to serum albumin. *Pharmacol Rev.* 1981; 33: 17–53. PMID: [7027277](#)
21. Cheruvallath VK, Riley CM, Narayanan SR, Lindenbaum S, Perrin JH. A quantitative circular dichroic investigation of the binding of the enantiomers of ibuprofen and naproxen to human serum albumin. *J Pharm Biomed Anal.* 1997; 15: 1719–1724. PMID: [9260668](#)
22. Sakai T, Yamasaki K, Sako T, Kragh-Hansen U, Suenaga A, Otagiri M. Interaction mechanism between IS, a typical uremic toxin bound to site II, and ligands bound to site I of human serum albumin. *Pharm Res.* 2001; 18: 520–524. PMID: [11451040](#)
23. Sawas AH, Pentyala SN, Rebecchi MJ. Binding of volatile anesthetics to serum albumin: measurements of enthalpy and solvent contributions. *Biochemistry.* 2004; 43: 12675–12685. PMID: [15449957](#)
24. Davilas A, Koupparis M, Macheras P, Valsami G. In-vitro study on the competitive binding of diflunisal and uraemic toxins to serum albumin and human plasma using a potentiometric ion-probe technique. *J Pharm Pharmacol.* 2006; 58: 1467–1474. PMID: [17132209](#)
25. Fanali G, Cao Y, Ascenzi P, Trezza V, Rubino T, Parolaro D, et al. Binding of  $\delta$ 9-tetrahydrocannabinol and diazepam to human serum albumin. *IUBMB Life.* 2011; 63: 446–451. doi: [10.1002/iub.466](#) PMID: [21557446](#)
26. Devine E, Krieter DH, R  th M, Jankovski J, Lemke HD. Binding affinity and capacity for the uremic toxin indoxyl sulfate. *Toxins.* 2014; 6: 416–429. doi: [10.3390/toxins6020416](#) PMID: [24469432](#)
27. Buller AR, Townsend CA. Intrinsic evolutionary constraints on protease structure, enzyme acylation, and the identity of the catalytic triad. *Proc Natl Acad Sci U. S. A.* 2013; 110: E653–E661. doi: [10.1073/pnas.1221050110](#) PMID: [23382230](#)
28. Yang F, Bian C, Zhu L, Zhao G, Huang Z, Huang M. Effect of human serum albumin on drug metabolism: structural evidence of esterase activity of human serum albumin. *J Struct Biol.* 2007; 157: 348–355. PMID: [17067818](#)
29. Liasova MS, Schopfer LM, Lockridge O. Reaction of human albumin with aspirin *in vitro*: mass spectrometric identification of acetylated lysines 199, 402, 519, and 545. *Biochem Pharmacol.* 2010; 79: 784–791. doi: [10.1016/j.bcp.2009.10.007](#) PMID: [19836360](#)
30. Bhattacharya AA, Curry S, Franks NP. Binding of the general anesthetics propofol and halothane to human serum albumin: high resolution crystal structures. *J Biol Chem.* 2000; 275: 38731–38738. PMID: [10940303](#)
31. Curry S. Lessons from the crystallographic analysis of small molecule binding to human serum albumin. *Drug Metab Pharmacokinet.* 2009; 24: 342–357. PMID: [19745561](#)
32. Sugio S, Kashima A, Mochizuki S, Noda M, Kobayashi K. Crystal structure of human serum albumin at 2.5 Å resolution. *Protein Eng.* 1999; 12: 439–446. PMID: [10388840](#)
33. Antonini E, Anderson SR. The binding of carbon monoxide by human hemoglobin: proof of validity of the spectrophotometric method and direct determination of the equilibrium. *J Biol Chem.* 1968; 243: 2918–2920. PMID: [5653184](#)
34. Kanto J, Iisalo E, Lehtinen V, Salminen J. The concentrations of diazepam and its metabolites in the plasma after an acute and chronic administration. *Psychopharmacologia.* 1974; 36: 123–131. PMID: [4407689](#)
35. Reidenberg MM, Levy M, Warner H, Coutinho CB, Schwartz MA. Relationship between diazepam dose, plasma level, age, and central nervous system depression. *Clin Pharmacol Ther.* 1978; 23: 371–374. PMID: [630787](#)
36. Rutherford DM, Okoko A, Tyrer PJ. Plasma concentrations of diazepam and desmethyldiazepam during chronic diazepam therapy. *Br J Clin Pharmacol.* 1978; 6: 69–73. PMID: [352377](#)
37. Tempero KF, Cirillo VJ, Steelman SL. Diflunisal: a review of pharmacokinetic and pharmacodynamic properties, drug interactions, and special tolerability studies in humans. *Br J Clin Pharmacol.* 1977; 1: 31S–36S. PMID: [328032](#)

38. Mojaverian P, Rocci ML Jr., Swanson BN, Vlasses PH, Chremos AN, Lin JH, et al. Steady-state disposition of diflunisal: once- versus twice-daily administration. *Pharmacotherapy*. 1985; 5: 336–339. PMID: [3841206](#)
39. Janssen GM, Venema JF. Ibuprofen: plasma concentrations in man. *J Int Med Res*. 1985; 13: 68–73. PMID: [3979659](#)
40. Laska EM, Sunshine A, Marrero I, Olson N, Siegel C, McCormick N. The correlation between blood levels of ibuprofen and clinical analgesic response. *Clin Pharmacol Ther*. 1986; 40: 1–7. PMID: [3522030](#)
41. Kanto J, Gepts E. Pharmacokinetic implications for the clinical use of propofol. *Clin Pharmacokinet*. 1989; 17: 308–326. PMID: [2684471](#)
42. Macquaire V, Cantraine F, Schmartz D, Coussaert E, Barvais L. Target-controlled infusion of propofol induction with or without plasma concentration constraint in high-risk adult patients undergoing cardiac surgery. *Acta Anaesthesiol Scand*. 2002; 46: 1010–1016. PMID: [12190804](#)
43. Khan MS, Zetterlund EL, Gréen H, Oscarsson A, Zackrisson AL, Svanborg E, et al. Pharmacogenetics, plasma concentrations, clinical signs and EEG during propofol treatment. *Basic Clin Pharmacol Toxicol*. 2014; 115: 565–570. doi: [10.1111/bcpt.12277](#) PMID: [24891132](#)
44. Stanfel LA, Gulyassy PF, Jarrard EA. Determination of indoxyl sulfate in plasma of patients with renal failure by use of ion-pairing liquid chromatography. *Clin Chem*. 1986; 32: 938–942. PMID: [3085981](#)
45. Ascenzi P, Gianni S. Functional role of transient conformations: rediscovering “chronosteric effects” thirty years later. *IUBMB Life*. 2013; 65: 836–844. doi: [10.1002/iub.1208](#) PMID: [24078391](#)
46. Pettersen EF, Goddard TD, Huang CC, Couch GS, Greenblatt DM, Meng EC, et al. UCSF Chimera—a visualization system for exploratory research and analysis. *J Comput Chem*. 2004; 25: 1605–1612. PMID: [15264254](#)